Materials Science & Engineering A 597 (2014) 431–439

Contents lists available at ScienceDirect

Materials Science & Engineering A

journal homepage: www.elsevier.com/locate/msea

Correlations between nanoindentation hardness and macroscopic mechanical properties in DP980 steels

M.D. Taylor [b], K.S. Choi [a], X. Sun [a,*], D.K. Matlock [b], C.E. Packard [b], L. Xu [c], F. Barlat [d]

[a] Pacific Northwest National Laboratory, P.O. Box 999, Richland, WA 99352, United States
[b] Colorado School of Mines, Golden, CO 80401, United States
[c] Leongjin Special Steel Co Ltd., Jintan City, Jiangsu Province, China
[d] GIFT-POSTECH, Pohang, Gyeongbuk 790-784, Republic of Korea

ARTICLE INFO

Article history:
Received 5 September 2013
Received in revised form
27 December 2013
Accepted 28 December 2013
Available online 6 January 2014

Keywords:
Nanoindentation
Dual phase
Constituent hardness
Hole expansion ratio

ABSTRACT

Nanoindentation measurements were obtained on eight commercially-produced DP980 dual-phase steels to quantify the hardness of the individual constituents, ferrite and martensite, in each steel. Each microstructure was also evaluated to determine grain size, martensite volume fraction (MVF), and retained austenite content. Nanoindentation hardnesses and quantitative microstructural measurements were correlated with tensile properties and performance in hole expansion tests to assess the importance of the individual constituent properties. Hole expansion samples were prepared with both sheared edges produced by mechanical punching, and non-deformed edges produced by electric discharge machining (EDM). Average material hardness based on nanoindentation data correlated directly to Vickers hardness measurements, verifying the capability of the nanoindentation technique to produce data consistent with traditional hardness measurements. Yield strength (YS) correlated directly to ferrite hardness indicating that, for a similar MVF and microstructural morphology, the YS is controlled by the strength of the softer matrix phase (ferrite). Hole expansion ratios (HER) on EDM samples decreased with an increase in both martensite and ferrite hardness, indicating that EDM HER values can be enhanced by softening both constituents. Punched-hole HER values decreased with increasing martensite hardness and martensite-to-ferrite hardness ratio, but were independent of ferrite hardness, indicating that softening the martensite while increasing the ferrite hardness could produce a higher HER.

1. Introduction

Advanced High Strength Steels (AHSS) are being increasingly used by the global automotive industry to cost-effectively reduce vehicle weight. AHSS micro-constituents can include retained austenite, bainite, ferrite, and martensite, combinations of which produce higher strengths compared to mild steels while still maintaining sufficient elongation [1,2]. Most AHSS products available are performance-based steels, e.g., user-defined criteria are specified by some basic mechanical property such as the minimum ultimate tensile strength (UTS), or yield ratio [3]. Steel makers can produce steels that meet a specific strength class by multiple different alloying and thermo-mechanical processing strategies, which correspond to potentially different microstructures. These variations in microstructure could affect formability performance in automotive manufacturing operations.

Based on current and planned usage, dual-phase (DP) steels represent the most important AHSS grade. DP steels contain primarily martensite and ferrite, and multiple DP grades can be produced by controlling the martensite volume fraction (MVF) [4]. DP steels are commercially available with UTS values up to 980 MPa (designated as DP980), and higher strength grades are under development. Within the DP980 strength class, steel producers offer focused modifications with enhanced specific characteristics, e.g. improved bending, stretch flangeability, or high yield ratio [3]. As a result, two steels of the same strength class can exhibit different performances during forming, believed to be in response to their respective microstructural constituent properties [2,5–10]. An area of interest for both steel producers and users is to develop a more complete understanding of the microstructural properties that influence local formability and fracture of AHSS.

Dual-phase steels are known to be sensitive to localized fracture [11], and traditional measures of ductility, such as total elongation (TE) obtained from a uni-axial tensile test, are often inaccurate indicators of local formability [8,12,13]. Laboratory measurements of hole expansion ratios (HER) are commonly utilized to represent

* Corresponding author. Tel.: +1 509 372 6489; fax: +1 509 372 6099.
E-mail address: xin.sun@pnnl.gov (X. Sun).

0921-5093/$ - see front matter © 2014 Elsevier B.V. All rights reserved.
http://dx.doi.org/10.1016/j.msea.2013.12.084

industrial forming operations, to evaluate in-die performance and to assess localized fracture [14]. Multiple studies have concluded that, with an increase in hardness disparity between constituents, HER properties are typically degraded [2,5–7,9–11,15–18].

Recently, different techniques have been employed to quantify the strength of individual constituents in DP steels, and the methods include Vickers hardness, calculations based on chemical content, micropillar compression, and nanoindentation. Owing to the fine grain sizes usually present in DP steels, techniques such as Vickers hardness, even when performed at the minimum load, are too large for the fine-scale microstructures [19,20]. Estimations of hardness based on chemical content inherently possess assumptions based on cooling rates and post-processing (i.e. temper rolling) that could lead to potential error, especially when considering the multitude of processing paths that can produce DP steels [16,21]. Micropillar compression tests are capable of generating stress–strain responses of individual constituents, which are valuable for finite element modeling (FEM) of microstructures [22]. However, the preparation, cost, time, and precision of micropillar compression can potentially make the technique prohibitive. Consequently, only a few micropillars of a DP steel can be tested in a reasonable amount of time, leading to a higher uncertainty when assigning data from only a few grains to an entire population. Many recent studies using nanoindentation have been performed on steels, and in some cases, hardness values of individual constituents were obtained [23–30]. Owing to the shallow depths associated with nanoindentation, multiple indentations within an individual grain can be obtained and averaged to determine an average individual constituent hardness [31]. Data obtained from nanoindentation have even been extended to indirectly measure strain-hardening exponents [32,33], besides reasonably predicting stress–strain curves [26].

The purpose of this study was to systematically evaluate, via nanoindentation testing, the hardness of the ferrite and martensite present in a series of commercially produced DP980 steels, and to correlate the measured hardness with macroscopic mechanical properties, including Vickers hardness, tensile properties, and hole expansion data.

2. Experimental procedure

2.1. Chemical composition

Table 1 summarizes the designation, thickness, and composition (in wt%) for each of the eight commercially produced DP980 steels used in this study. All steels in this study were tested in the as-received condition for the following experiments.

2.2. Microstructural property characterizations

2.2.1. Grain size and volume fraction analysis

Ferrite and martensite grain sizes were quantified based on the measurement method for a two-phase microstructure developed by Higginson and Sellars [34]. For analysis, five micrographs were taken at random locations from both the in-plane and transverse orientations using a field-emission scanning electron microscope (SEM), resulting in 10 micrographs. The metallographic samples were prepared using standard techniques and polished to a 1 μm diamond finish followed by etching in 2% nital (2% nitric acid, in ethanol) for approximately 10 s. Three concentric circles with 60 proportionally spaced tick marks were overlaid onto each micrograph. The locations of the tick marks were used to determine phase fractions with standard point counting methods and the boundary/circle intercepts were used to determine grain sizes by separately identifying and counting ferrite/ferrite (f/f) boundary intersections and ferrite/martensite (f/m) boundary intersections. A more detailed explanation of the procedure can be found elsewhere [35]. Average ferrite and martensite grain sizes were calculated based on Eqs. (1) and (2), respectively,

$$L_\alpha = \frac{(1 - V_{f-\alpha'}) \times L}{(n_\alpha + 0.5 n_{\alpha'})} \tag{1}$$

$$L_{\alpha'} = \frac{(2 \times V_{f-\alpha'}) \times L}{n_{\alpha'}} \tag{2}$$

where $V_{f-\alpha'}$ is the local MVF, L is the total length of the circles used, n_α is the number of f/f counts, and $n_{\alpha'}$ is the number of f/m counts per measurement field. Each micrograph was analyzed twice, with the concentric circle overlay randomly located in two positions, resulting in 20 measurement fields. The 20 measurement fields resulted in over 2000 boundary counts and 1200 MVF counts for each steel. Averages of the 20 ferrite grain size, martensite grain size, and MVF data points were calculated.

2.2.2. X-ray diffraction

Retained austenite content was evaluated using x-ray diffraction (XRD) on the rolling plane of samples which were mechanically ground and chemically polished in a solution of 1 part hydrofluoric acid, 10 parts hydrogen peroxide, and 10 parts de-ionized water for approximately 5 min. Chemical polishing removed surface deformation induced by mechanical polishing methods, which can potentially transform the austenite at the surface to martensite and misrepresent the austenite present in the steel. Copper K_α radiation was used on samples scanned through a 2-theta from 35–105°. Measured retained austenite content in all steels was low, and thus amounts were referenced to the austenite detection resolution limit of approximately 3% by volume. Specifically, steels were characterized as either to contain detectable limits (identified "yes" in Section 3) or to exhibit levels that were undetectable (identified "no").

2.2.3. Nanoindentation

Nanoindentation tests were performed using a Hysitron® TI950 Triboindenter on unetched samples prepared with the same procedure used for metallographic analysis in Section 2.2.1 with the addition of a final 0.05 μm colloidal silica vibratory polishing step. The resulting sample roughness was 4–10 nm. All nanoindentation tests were performed using a Berkovich indenter tip operated in displacement-control to a depth of 40 nm with a 20 nm/s loading rate, hold for 2 s, and unloaded at 20 nm/s. A 15 × 15 array of indentations (225 total) was performed on each sample, and hardness values were calculated using the Oliver–Pharr method [36]. An indentation spacing of 2 μm was chosen to eliminate potential effects of overlapping plastic zones [37]. After indentation, the tested areas were imaged using a SEM, and an example of the resulting micrograph for steel A is shown in Fig. 1a. A transparent film was placed on the SEM micrograph in Fig. 1a to record the location of each indentation. The samples were then etched with 2% nital to reveal the microstructure. Each sample was

Table 1
Chemistry (in wt%) of the eight DP980 steels used in this study.

Steel	Thickness (mm)	C	Mn	Si	Ni	Cr	Mo	Ti	Nb	Cu
A	2	0.09	2.13	0.57	0.01	0.02	0.07	0.02	0.009	0.07
B	1.7	0.09	2.16	0.31	0.01	0.20	0.27	0.02	0.015	0.01
C	1	0.11	2.38	0.08	0.01	0.26	0.20	0.04	0.031	0.01
D	1.2	0.12	2.47	0.03	<0.01	0.25	0.36	0.01	0.002	0.01
E	2	0.09	2.10	0.33	0.01	0.46	0.29	0.05	0.036	0.01
F	1.4	0.10	2.09	0.18	0.01	0.47	0.28	0.03	0.017	0.01
G	1.4	0.08	2.08	0.18	0.01	0.47	0.28	0.03	0.017	0.01
H	1	0.15	1.93	0.64	0.04	0.32	0.01	0.13	0.003	0.04

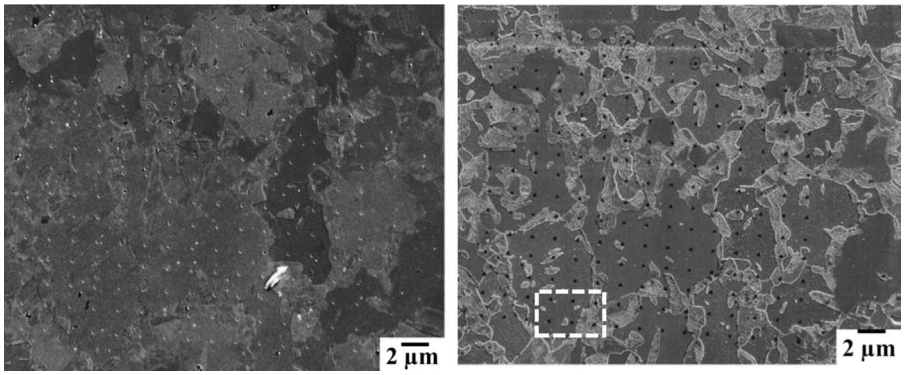

Fig. 1. SEM micrograph of the polished surface of steel A steel with indents in (a), and SEM micrograph of the same area with an etched surface and the indent overlay in (b). Etched with nital for approximately 10 s.

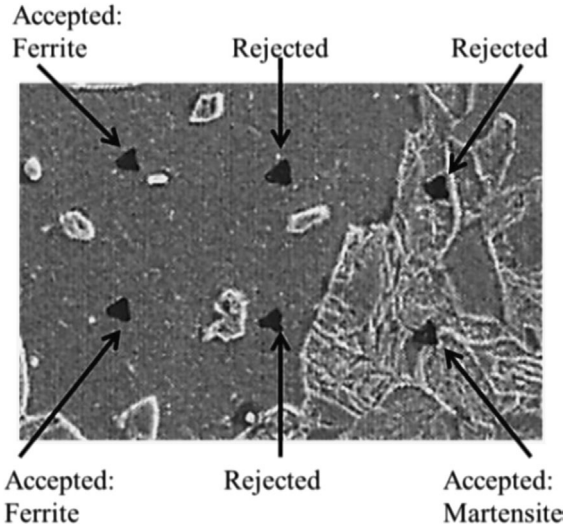

Fig. 2. Magnified view of the dashed box in Fig. 1b that illustrates whether indents were accepted or rejected according to the criteria explained in the text.

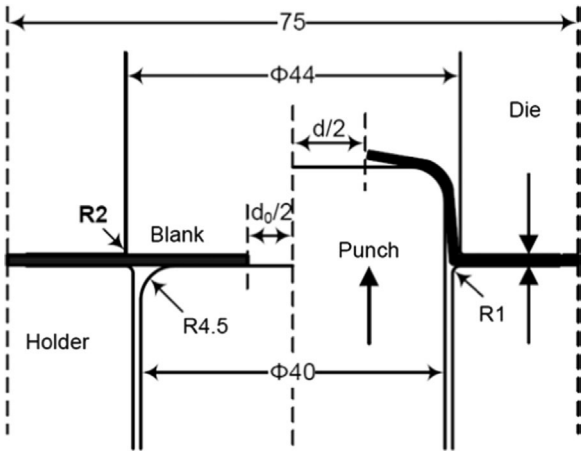

Fig. 3. Schematic of hole expansion test setup using a flat-bottomed punch. All dimensions in mm [12].

placed back in the SEM, and the same area was imaged at the same magnification as the polished surface with the indentations. After etching, most indentations were not visible, and thus the transparent film was placed over the etched SEM micrograph to locate the indentations, using visible indents for alignment. A resulting final image is shown in Fig. 1b.

Each indentation was categorized as located in either ferrite or martensite, or was discarded due to proximity to an interface boundary visible on the micrograph. Indentations within 1.5 indent diameters from an interface were discarded from the data so that potential constraining effects of the interface and dissimilar adjacent material were removed [37]. An illustration of six indentations that were either rejected or accepted is shown in Fig. 2 for a magnified view of the region in the dashed white box in Fig. 1b. After removing indentation data within 1.5 indent diameters from interfaces, the remaining ferrite and martensite data were separately averaged to obtain hardness values for the individual constituents in each steel.

2.2.4. Vickers hardness

To relate data generated from nanoindentation to a standardized measuring technique, Vickers hardness data were obtained using a 300 g mass, and a dwell time of 10 s. Vickers hardness data were chosen to observe correlations with nanoindentation because the Berkovich and Vickers indenter tips have equivalent contact area-to-depth ratios [38]. Ten Vickers indentations were randomly placed on each steel, and the ten Vickers hardness values were averaged.

2.3. Mechanical properties

ASTM E-8 sub-sized tensile samples with a reduced gauge length of 32 mm X 6 mm X sheet thickness were prepared by electric discharge machining (EDM) with the rolling direction parallel to the tensile axis [39]. Tests were performed on a universal servo-hydraulic testing system at a strain rate of 10^{-4}/s. A 25.4 mm extensometer was used to monitor strain in the gauge section. Three samples were tested for each steel, and the properties of yield strength (YS), UTS, uniform elongation (UE) and TE were obtained from the average of the three tests. Values for YS were obtained using a 0.2% strain offset.

Hole expansion samples, 75×75 mm^2, were cut from each DP980 steel. A hole with 12 mm diameter was created in the center of each sample, both by punching, representing industrial practice, and by EDM. Fig. 3 shows a schematic of the hole expansion test setup, which included a 40 mm diameter, 4.5 mm radius flat-bottomed punch. Tests were performed at a punch displacement rate of 20 mm/min with a die holding force of 100 kN. For punched-hole samples, tests were performed with the sheared lip oriented upwards. Each test was stopped when the first crack adjacent to the hole was visually detected. Three tests were performed for each hole preparation method. The final hole

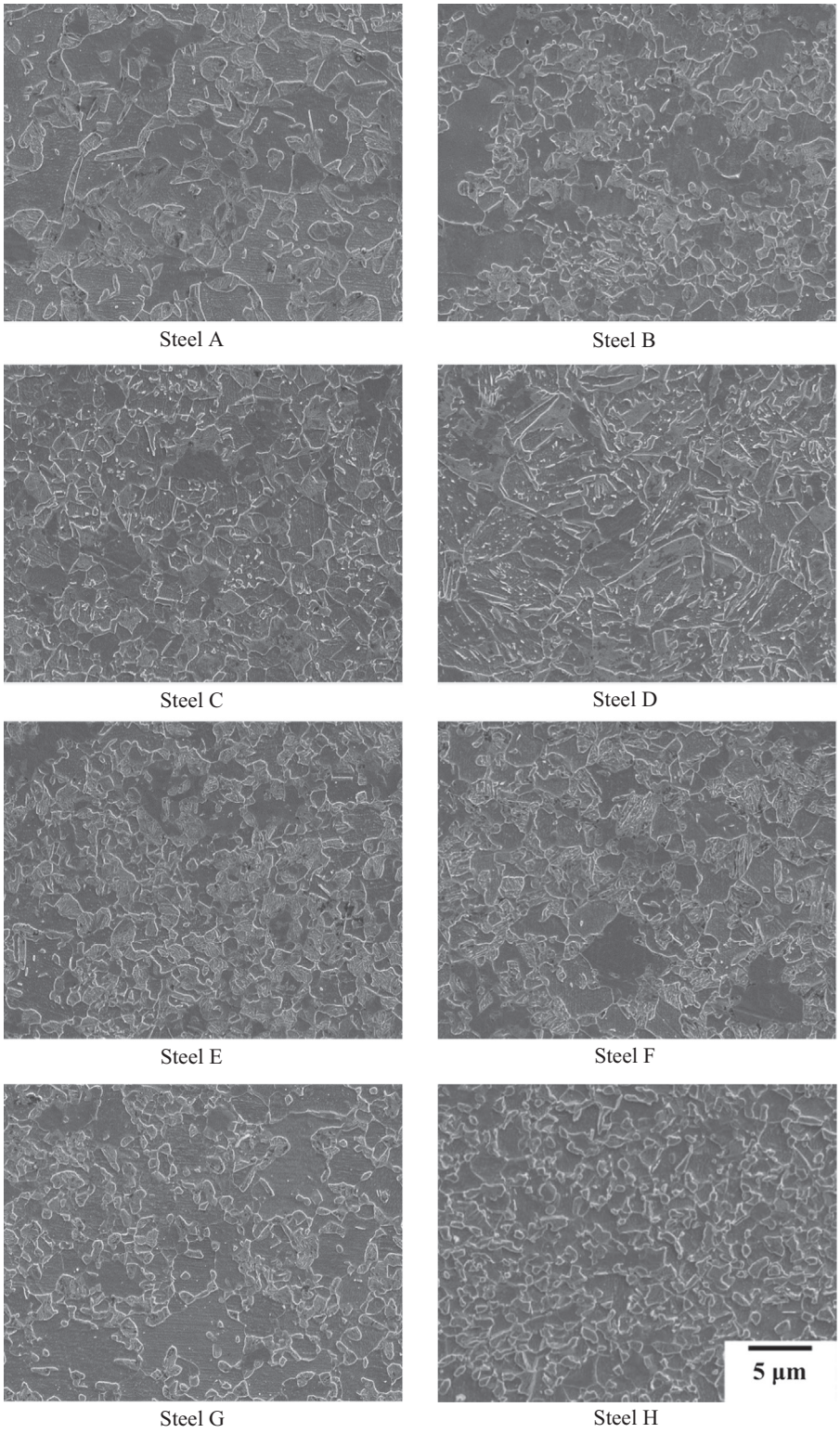

Fig. 4. SEM micrographs for steels A–H taken from the in-plane orientation. All steels were etched with nital for approximately 10 s. All steels appear to exhibit an equiaxed morphology, except for steel D, which appears to contain low-temp products.

diameter, d, was measured, and the HER was calculated using Eq. (3),

$$\text{HER} = \frac{d - d_o}{d_o} \times 100\% \quad (3)$$

where d_o is the initial diameter. The three HER values obtained for each hole preparation method were averaged.

3. Results

3.1. Microstructural analysis

Fig. 4 presents SEM micrographs from the in-plane orientation for the eight DP980 steels. All steels except steel D exhibited relatively equiaxed microstructures, with steel A exhibiting the

Table 2
Measured microstructural and macroscopic mechanical properties of interest for all eight steels.

Steel grade	Y.S. (MPa)	UTS (MPa)	UE (%)	TE (%)	Hardness, α (GPa)	Hardness, α' (GPa)	α'/α	Avg. hardness (GPa)	Vickers hardness
A	689	1000	8.2	15	3.85	6.76	1.76	5.2	303
B	682	1024	8.2	15.1	3.88	8.3	2.14	5.5	316
C	769	1084	5.9	12.4	4.57	8.52	1.86	6.6	336
D	727	984	6.8	12.5	4.45	9.25	2.08	5.1	311
E	665	1020	8.9	16.8	3.84	7.06	1.84	4.9	314
F	663	1007	8.8	17.3	3.75	7.05	1.88	4.8	303
G	665	993	9.7	17.1	4.02	8.52	2.12	5.1	313
H	558	983	13.5	19.7	3.33	8.67	2.60	4.2	290

Steel grade	Grain size, α (μm)	Grain size, α' (μm)	MVF (%)	HER punch (%)	HER EDM (%)	Austenite
A	1.82	1.09	32.5	25.2	38.1	No
B	1.42	0.88	30	18.4	26.6	No
C	1.47	0.88	31	14.9	16.9	No
D	1.45	0.81	28	17.2	19.0	Yes
E	1.19	0.89	35	16.8	32.7	No
F	1.38	1	36	23.3	26.6	No
G	1.37	0.82	31	13.5	25.6	No
H	1.18	0.6	26.3	14.3	26.5	Yes

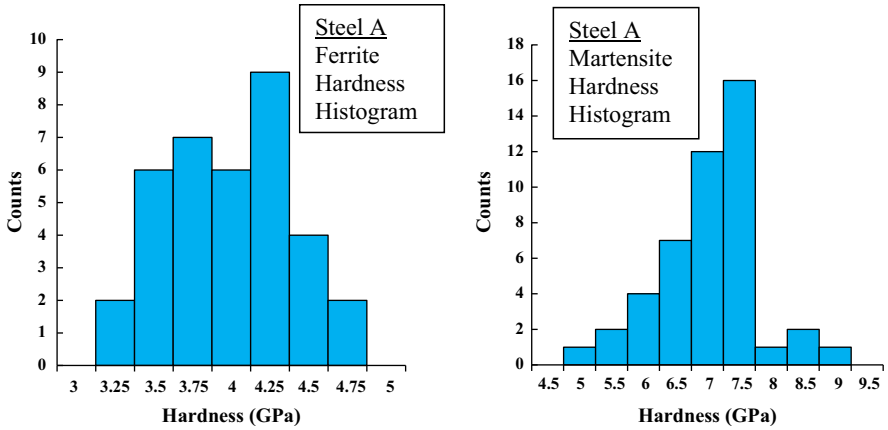

Fig. 5. Hardness histograms of steel A for ferrite in (a), showing a normal distribution, and for martensite in (b), showing a skewed-left distribution.

largest ferrite grain size, and steel H exhibiting the finest ferrite grain size. The microstructure of steel D is non-equiaxed, and is interpreted to exhibit low transformation temperature products, possibly a result of having the highest molybdenum content (0.36 wt%) in this study. Very fine, acicular laths can be observed in steel D, and some are interpreted to be retained austenite.

Table 2 summarizes the quantitative microstructural data for all steels in this study. The steels exhibited fine microstructures with average ferrite (α) grain sizes between 1.2 and 1.8 μm, average martensite (α') island sizes between 0.6 and 1.1 μm, and MVF between 26% and 36%. Only steels D and H contained observable amounts of retained austenite based on XRD data.

3.2. Hardness test: nanoindentation and Vickers

Fig. 5 presents histograms of hardness values obtained for Steel A (selected as an example data set), with the distribution of ferrite hardness values in Fig. 5a and the martensite values in Fig. 5b. The observed range of hardness values for each constituent in Fig. 5 may reflect an inhomogeneous distribution of chemical content within grains, dislocation density variations within grains, and/or potential contributions of the microstructure below the indented plane. The ferrite data in Fig. 5a approximate a normal distribution, an observation consistent with most hardness distributions in this study. Thus, averages of constituent hardness values are summarized in Table 2, and the range of values are consistent with average ferrite and martensite hardness values reported by others [23–27,29,30]. In a limited number of cases, the hardness distribution appeared skewed, as illustrated in Fig. 5b. In all steels, ferrite and martensite hardness data separated into two distinct groups.

To observe the overall average material hardness as measured by nanoindentation, the average of all 225 nanoindentations for each steel is reported in Table 2. Note that this average calculation included data points near interfaces, which were excluded in the calculations for individual constituent hardness values. Although some studies relate the hardness difference between constituents to formability [11,18], an alternate parameter assessed here is the martensite-to-ferrite (m/f) hardness ratio, also summarized in Table 2. The m/f hardness ratio for all steels in this study ranged between 1.8 and 2.6, and Vickers hardness data ranged from 290 to 336 VHN in Table 2.

3.3. Tensile properties

Fig. 6 shows representative stress–strain curves for steels B and H. Steel B, selected as representative of steels A–G, exhibited continuous yielding, characteristic of DP steels [2,40]. In contrast, steel H presents a stress–strain behavior which exhibited the lowest YS, a region where the strain hardening rate increased with strain (indicated by the arrow), and the highest TE. The work hardening behavior of steel H is similar to that of transformation-induced plasticity (TRIP) steel [2], and the observed behavior is

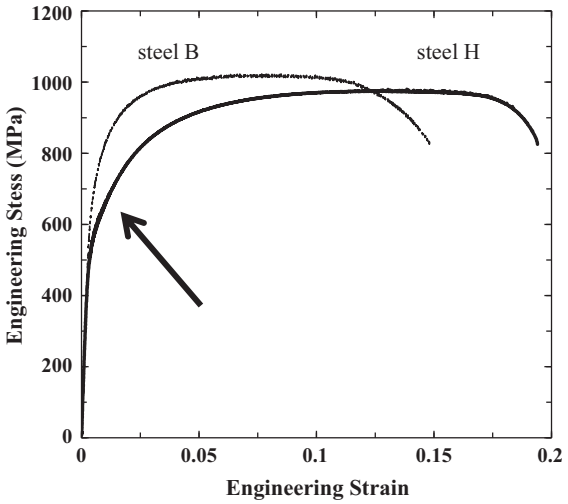

Fig. 6. Engineering stress–strain curve for steels B and H. Steel B was chosen to represent the stress–strain response of steels A–G since all exhibited similar strain hardening characteristics. All steels achieve a UTS greater than 980 MPa.

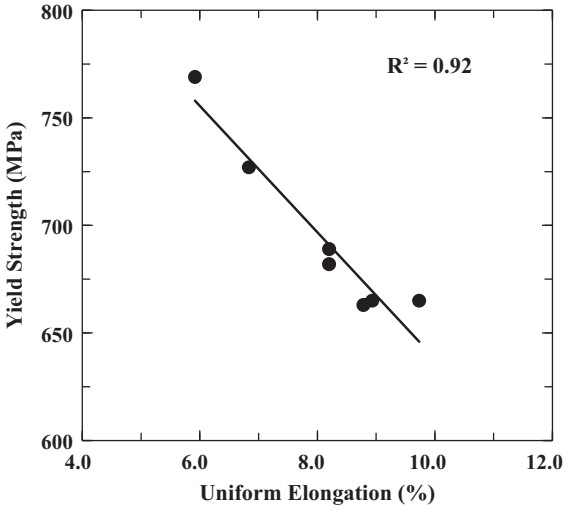

Fig. 7. Correlation of YS versus UE for steels A–G. A decreasing, linear trend exists that suggests that for a similar strain-hardening behavior, UE is dependent on YS.

supported by the presence of retained austenite measured using XRD. Though XRD also indicated a detectable amount of austenite in steel D, its stress–strain curve is very similar to those of steels A, B, C, E, F, and G, suggesting that the volume fraction of retained austenite may be insufficient to impact the mechanical response in uni-axial tension. Fig. 7 summarizes stress–strain data by correlating YS with UE, and a strong linear correlation is observed for steels A–G. From previous studies on DP steels [40], a trend similar to Fig. 7 was observed for steels with different yield strengths, but with very similar strain-hardening behavior. The relationship in Fig. 7 supports the assumption that the stress–strain curve of steel B is representative of steels A–G. Summarized in Table 2 are the YS, UTS, UE, and TE for all steels in this study, all achieving the minimum grade requirement of UTS values above 980 MPa.

3.4. Hole expansion

Fig. 8 shows an example of a tested hole expansion sample for steel A in which the initial crack formed parallel to the rolling direction. The behavior shown in Fig. 8 is characteristic of all steels in this study, and crack initiation locations were either parallel or

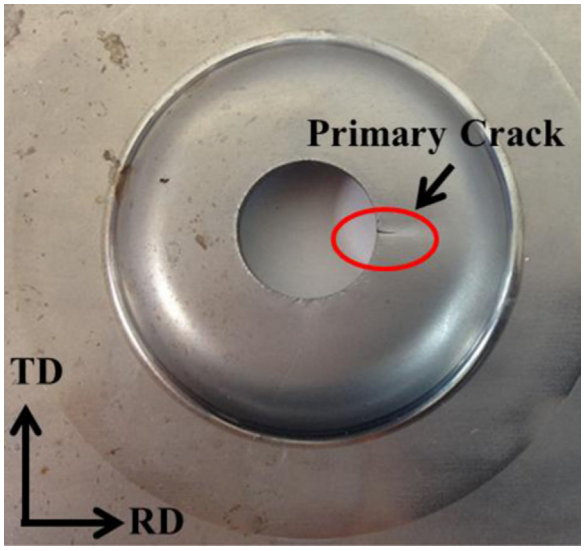

Fig. 8. Light optical photo of a tested hole expansion sample of steel A in the punched condition. In this case, the "Primary Crack" formed parallel to the rolling direction. Figure adapted from Choi et al. [12].

transverse to the rolling direction, the specific orientation independent of the steel being tested. The resulting HER data are summarized in Table 2. A low variability between HER values was observed, and HER values for samples with holes prepared by EDM were consistently higher than that for samples with punched holes, indicating the shear damage induced by the punch process has a negative impact on the subsequent hole stretchability [11,21,41].

4. Discussion

Selected correlations are presented to illustrate the observed relationships between microstructural and mechanical properties. Also, a correlation between nanoindentation data and Vickers hardness data is explored. All potential relationships are evaluated with either a linear or power function, and the degree of fit is determined by the correlation coefficient, R^2. Plots with R^2 values greater than 0.3 are categorized as potential relationships. In all cases, the R^2 values are reported in the figures.

Fig. 9 correlates the average material hardness obtained from nanoindentation with Vickers hardness measurements. A strong linear correlation is observed, which verifies the ability of nanoindentation to produce results consistent with Vickers hardness tests, and subsequent categorization of the nanoindentation data into ferrite and martensite with the method outlined in Section 2.2.4 is interpreted to accurately represent the relative hardness values of constituents. The equivalent contact area-to-depth ratios of Vickers and Berkovich indenters are interpreted to contribute to the quality of the linear correlation in Fig. 9. Correlations between categorized hardness values and mechanical properties are discussed below.

For all steels in this study, the MVF ranged from 26 to 36% indicating that ferrite is the dominant, matrix phase. From previous studies on deformation of DP steels, ferrite is known to accommodate the majority of strain, and martensite the majority of stress [42–44]. Fig. 10 shows the YS versus average ferrite hardness, and a positive linear correlation is observed. The correlation in Fig. 10 is consistent with the interpretation of two-constituent composites in which the lower-strength constituent (ferrite in DP steel) controls the onset of yielding [45]. Material YS obtained from a tensile test is considered a global property in the

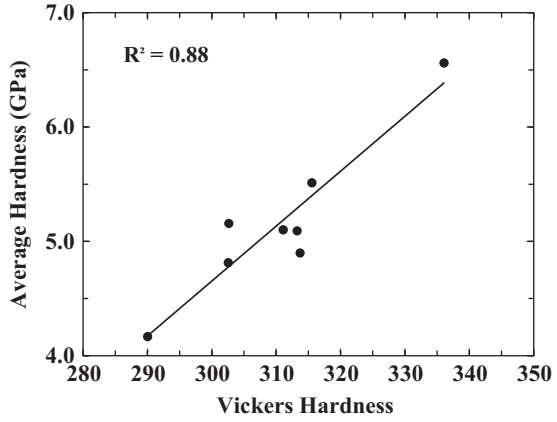

Fig. 9. Correlation of average nanoindentation data to Vickers hardness data, indicating a linear relationship between data obtained using nanoindentation and Vickers.

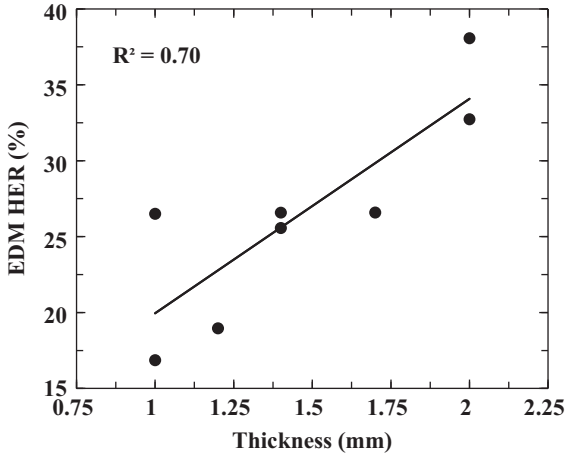

Fig. 11. Correlation of EDM HER to sheet thickness, indicating that HER increases with thicker sheets, and is consistent with the literature.

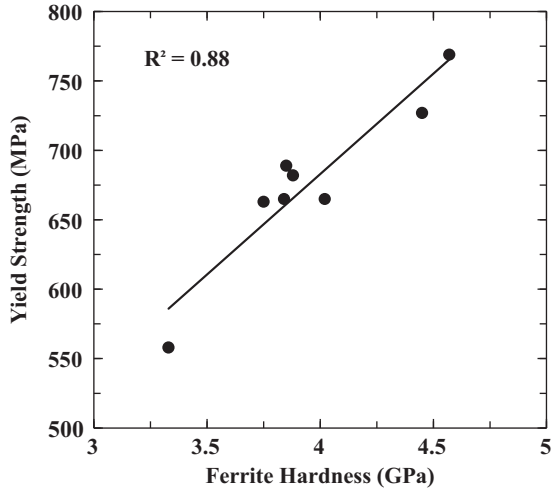

Fig. 10. Correlation of YS versus ferrite hardness, indicating that for a similar MVF and microstructural morphology, the yielding behavior of steels is controlled by the softer, matrix phase.

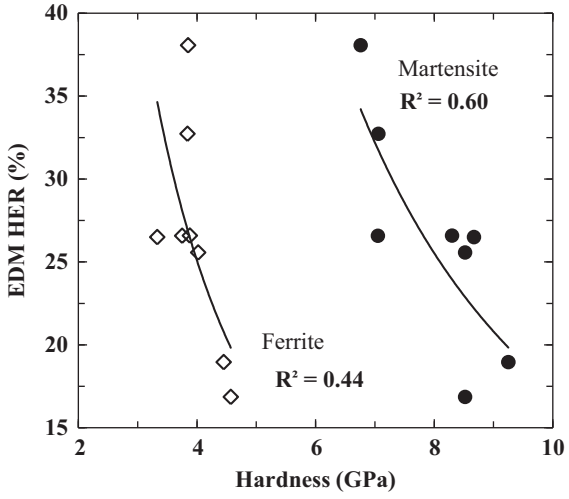

Fig. 12. Correlation of EDM HER to ferrite and martensite hardness. The correlations were created using a power law function, and show that decreasing both constituent hardness values lead to an increase in HER.

sense that mechanisms present at the scale of the entire sample are considered [11]. In contrast, hole expansion tests are governed by local properties, where only a few grains adjacent to the hole are considered.

Fig. 11 shows a plot of EDM HER versus steel thickness, and the observed positive linear correlation indicates that the resistance to failure in HER testing may increase with thicker sheets [46]. Specifically, material thinning at the hole periphery is the primary failure mechanism during hole expansion testing, and it is interpreted that thicker steels will require additional thinning in order to fail [47]. Further study of thickness effects is warranted and it is suggested that a systematic study of reducing a sheet thickness and obtaining HER values for a specific steel grade and hole diameter would provide further insight.

Fig. 12 shows EDM HER versus ferrite and martensite hardness, and for both constituents, EDM HER decreases with an increase in hardness. Fig. 12 indicates that the individual hardnesses of ferrite and martensite may contribute independently to EDM HER. The relationship in Fig. 12 is supported by the relatively narrow range of MVF, because such a relationship would be unexpected if there were significant differences in MVF between the steels in this study. A qualitative analysis of the micrographs in Fig. 4 indicates that microstructural morphologies are similar (except steel D), which has been stated to have a greater effect on HER than the grain size [5–8,10]. Specifically, ferrite grains surrounded by an interconnected necklace of martensite would inhibit premature localized shear bands to persist over long distances in ferrite [8]. Because of the absence of a sheared edge, Fig. 12 indicates that constituent hardness can correlate to EDM HER in a similar way that constituent hardness can correlate to tensile properties (i.e. Fig. 10). Figs. 10 and 12 suggest that constituent hardness values can define mechanical properties, irrespective of whether fracture mechanisms are global (tensile) or localized (HER).

The EDM HER, compared to punched-hole HER, can be viewed as being more representative of the microstructural response since the shear-affected zone is absent. However, punched holes are more commonly encountered in industrial applications, and there is interest as to whether microstructural properties correlate to punched-hole HER. Fig. 13 shows that punched-hole HER decreases with increasing martensite hardness. Figs. 12 and 13 suggest, for a similar MVF and microstructural morphology, decreasing the martensite hardness will increase HER. Caution must be exercised when relating constituent hardness values from Table 2 to punched-hole HER, because constituent hardness values in Table 2 are representative of the ferrite and martensite hardness values in the as-received condition. After shearing, the localized plastic deformation in the region adjacent to the hole edge will alter the ferrite and martensite hardness. When considering HER,

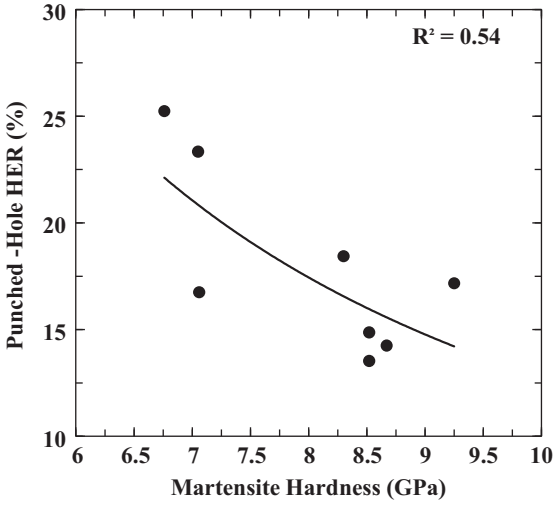

Fig. 13. Correlation of punched-hole HER to martensite hardness. The correlation was created using a power law function, and indicates with decreasing martensite hardness, punched-hole HER increases.

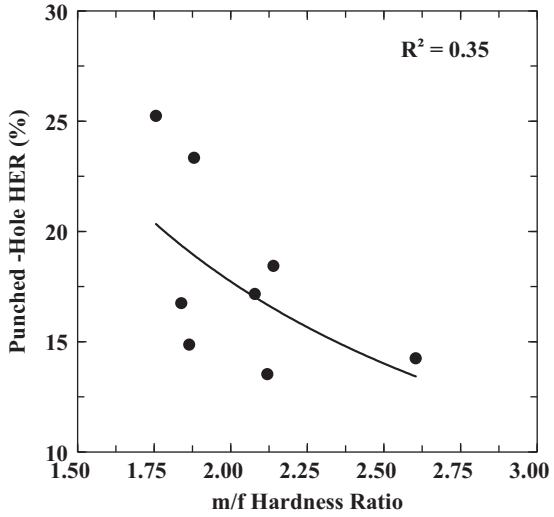

Fig. 14. Correlation of punched-hole HER to m/f hardness ratio. The correlation was created using a power law function, and indicates with increasing m/f hardness ratio, the damage imparted to the microstructure in the localized shear zone prior to testing increases.

localized fracture mechanisms are present, meaning that the properties of the highly deformed grains in close proximity to the hole edge will affect HER to a greater extent than the properties of the grains further away from the sheared edge (as-received condition). The reported HER data reflect the hardness values of the ferrite and martensite constituents in the sheared zone adjacent to the hole edge, and as a result EDM HER values are consistently higher than punched-hole HER for each steel. When considering the strain-hardening behavior of ferrite and martensite, ferrite was expected to strain-harden to a higher degree than martensite, and as a consequence, punched-hole HER values are essentially independent of the as-received ferrite hardness. In contrast, martensite was expected to experience limited strain-hardening during shearing, and the as-received martensite hardness still correlates with punched-hole HER values.

Fig. 14 shows a decreasing trend when punched-hole HER is plotted against the m/f hardness ratio. A higher m/f hardness ratio denotes a greater strength disparity between ferrite and martensite, which can cause a higher degree of strain localization at interfaces, leading to a higher density of void formation during deformation [42]. Taylor reported a positive correlation between void density and hardness ratio for a group of DP780 and DP980 steels deformed under a triaxial stress state [35], and this finding is supported by other studies that observed damage nucleation to occur at lower strains in DP steels with higher hardness differences between constituents [6]. Similar to Fig. 13, Fig. 14 correlates data from Table 2 (as-received hardness data), and shows that punched-hole HER decreases as the m/f hardness ratio increases. A greater m/f hardness ratio indicates a higher degree of strain partitioning to the softer ferrite phase, potentially inducing more damage to the matrix (shear bands, initial voids, etc.). Thus, a higher m/f hardness ratio will likely produce a sheared zone with greater ferrite damage before hole expansion testing, resulting in a lower HER.

In this study, HER values were observed to be independent of MVF, possibly due to the relatively narrow range of MVF for all steels in this study. Some researchers have concluded that an increased MVF may improve HER without any adverse effects [15,16,48], and have shown that a fully martensitic steel, when compared with two DP980 steels, exhibited a higher HER [16]. Other studies have concluded that as microstructures approach a single-phase composition, HER increases [49]. When the hardness ratio is 1 (i.e. fully martensitic), HER is higher than for DP980 steels, which inherently have hardness ratios greater than 1 (Fig. 14). This indicates that a minimization of the variation in strength between phases in a microstructure may be the dominant parameter affecting HER. Based on Figs. 12–14, increased HER values can be obtained by decreasing the martensite hardness and by increasing MVF.

5. Summary and conclusion

The microstructural properties of grain size, MVF, retained austenite, and constituent hardness were evaluated and used to assess correlations with the macroscopic mechanical properties of eight commercially produced DP980 steels. A positive correlation was observed between the average material hardness obtained using nanoindentation and Vickers hardness, verifying the capability of the nanoindentation technique to produce data consistent with traditional measurements of hardness. Nanoindentation measurements, when subsequently categorized into ferrite and martensite hardness values using the method outlined, exhibited correlations with select macroscopic mechanical properties. The positive correlation between ferrite hardness and YS suggests that, for a similar MVF and microstructural morphology, the YS is controlled by the strength of the softer matrix phase (ferrite).

The decreasing correlation between EDM HER and constituent hardness indicates that softening both phases will increase HER. However, increasing HER by simply softening the phases will also decrease the UTS, potentially changing the strength grade of the steel. A positive correlation was observed between EDM HER and sheet thickness, and is consistent with the current literature. Since multiple properties vary between all steels in this study, an experiment that maintains constant sheet thickness will better represent the effects of microstructural properties on HER. Decreasing correlations were observed when punched-hole HER was plotted against both martensite hardness and the m/f hardness ratio, indicating that softening the martensite could produce a higher HER. The punched-hole HER values are a product of the ferrite and martensite hardness values of the grains within the sheared zone adjacent to the hole, so caution should be used when interpreting punched-hole HER with the as-received ferrite and martensite hardness values reported in this study. Obtaining average ferrite and martensite hardness values in the as-received

condition, as well as in the sheared zone will be beneficial in observing the strain-hardening of both constituents, because it will allow for more accurate hardness–HER correlations, and will provide more robust data for the design of higher-HER steels without sacrificing strength. A suggested method to increase HER, while still maintaining a similar UTS, is to simultaneously decrease martensite hardness and increase ferrite hardness, thus maintaining a similar average hardness, while also lowering the hardness ratio between constituents.

Acknowledgments

Pacific Northwest National Laboratory is operated by Battelle Memorial Institute for the U.S. Department of Energy under Contract no. DE-AC06-76RL01830. This work was funded by the Department of Energy Office of FreedomCar and Vehicle Technologies under the Automotive Lightweighting Materials Program managed by Mr. William Joost. The suppliers and point of contacts who participated in this study are gratefully acknowledged for providing materials and support.

References

[1] R. Kuziak, R. Kawalla, S. Waengler, Arch. Civ. Mech. Eng. 8 (2008) 103–117.
[2] O. Kwon, K. Lee, G. Kim, K. Chin, Mater. Sci. Forum 638 (2010) 136–141.
[3] N. Pottore, N. Fonstein, I. Gupta, D. Bhattacharya, AHSSS Proc. (2004) 119–129.
[4] R.G. Davies, Metall. Trans. A 9 (1978) 671–679.
[5] J.H. Kim, M.G. Lee, D. Kim, D.K. Matlock, R.H. Wagoner, Mater. Sci. Eng. A 527 (2010) 7353–7363.
[6] G. Rosenberg, I. Sinaiová, Ľ. Juhar, Mater. Sci. Eng. A 582 (2013) 347–358.
[7] N. Saeidi, A. Ekrami, Mater. Sci. Eng. A. 523 (2009) 125–129.
[8] Y.M. Miura, M. Nakaya, Kobelco Technol. Rev. 28 (2008) 8–12.
[9] C.C. Tasan, J.P.M. Hoefnagels, M.G.D. Geers, Scr. Mater. 62 (2010) 835–838.
[10] J. Kadkhodapour, A. Butz, S. Ziaei Rad, Acta Mater. 59 (2011) 2575–2588.
[11] F. Hisker, R. Thiessen, T. Heller, Mater. Sci. Forum 706 (2012) 925–930.
[12] K.S. Choi, A. Soulami, D. Li, X. Sun, M. Khaleel, L. Xu, F. Barlat, Relationship between Material Properties and Local Formability of DP980 Steels, SAE Technical Paper no. 2012-01-0042, 2012, http://dx.doi.org/10.4271/2012-01-0042.
[13] T.M. Link, G. Chen, Assoc. Iron Steel Technol. (2013) 63–70, The Proceedings of the International Symposium on New Developments in Advanced High-Strength Sheet Steels, Vail, Colorado, USA, June 23–27, 2013, sponsored by "Association for Iron & Steel Technology".
[14] J. Dykeman, Assoc. Iron Steel Technol. (2013) 15–28, The Proceedings of the International Symposium on New Developments in Advanced High-Strength Sheet Steels, Vail, Colorado, USA, June 23–27, 2013, sponsored by "Association for Iron & Steel Technology". Developments in Advanced High-Strength Sheet Steels, Vail, Colorado, USA, June 23–27, 2013, sponsored by "Association for Iron & Steel Technology".
[15] S. Sagadopan, N. Ramisetti, H. Yao, MS&T Conference Proceedings, 2010, pp. 1–12.
[16] K. Hasegawa, K. Kawamura, T. Urabe, Y. Hosoya, ISIJ Int. 44 (2004) 603–609.
[17] K. Sugimoto, J. Kobayashi, D.V. Pham, Assoc. Iron Steel Technol. (2013) 175–184, The Proceedings of the International Symposium on New Developments in Advanced High-Strength Sheet Steels, Vail, Colorado, USA, June 23–27, 2013, sponsored by "Association for Iron & Steel Technology".
[18] M.S. Walp, A. Wurm, J.F. Siekirk, A.K. Desai, Shear Fracture in Advanced High Strength Steels, SAE Technical Paper no. 2006-01-1433, 2006, http://dx.doi.org/10.4271/2006-01-1433.
[19] R.D.K. Misra, S.W. Thompson, T.A. Hylton, A.J. Boucek, Metall. Mater. Trans. A. 32A (2001) 745–760.
[20] C. Chiriac, D. Hoydick, Assoc. Iron Steel Technol. (2013) 55–61, The Proceedings of the International Symposium on New Developments in Advanced High-Strength Sheet Steels, Vail, Colorado, USA, June 23–27, 2013, sponsored by "Association for Iron & Steel Technology".
[21] K. Takashima, Y. Toji, K. Hasegawa, MS&T Conference Proceedings, 2013, pp. 201–208.
[22] J.J. Williams, J.L. Walters, M.Y. Wang, N. Chawla, A. Rohatgi, J. Mater. 65 (2013) 226–233.
[23] Q. Furnemont, M. Kempf, P.J. Jacques, M. Goken, F. Delannay, Mater. Sci. Eng. A 328 (2002) 26–32.
[24] J. Moon, S. Kim, J. Jang, J. Lee, C. Lee, Mater. Sci. Eng. A 487 (2008) 552–557.
[25] T. Ohmura, K. Tsuzaki, J. Mater. Sci. 42 (2007) 1728–1732.
[26] B.W. Choi, D.H. Seo, J.Y. Yoo, J. Jang, J. Mater. Res. 24 (2009) 816–822.
[27] T. Ohmura, K. Tsuzaki, F. Yin, Mater. Trans. 46 (2005) 2026–2029.
[28] K.R. Gadelrab, G. Li, M. Chiesa, T. Souier, J. Mater. Res. 27 (2012) 1573–1579.
[29] R. Rodriguez, I. Gutierrez, Mater. Sci. Eng. A. 361 (2003) 377–384.
[30] K. Hayashi, K. Miyata, F. Katsuki, T. Ishimoto, T. Nakano, J. Alloy Compd. 577 (2013) S593–S596.
[31] M. Delince, P.J. Jacques, T. Pardoen, Acta Mater. 54 (2006) 3395–3404.
[32] M. Dao, N. Chollacoop, K.J. Van Vliet, T.A. Venkatesh, S. Suresh, Acta Mater. 49 (2001) 3899–3918.
[33] J.-Y. Kim, S.-K. Kang, J.R. Greer, D. Kwon, Acta Mater. 56 (2008) 3338–3343.
[34] R.L. Higginson, C.M. Sellars, Worked Examples in Quantitative Metallography, 1st ed., Maney Publishing, London (2003) 54–56.
[35] M.D. Taylor, Effect of microstructure on the fracture response of AHSS, Colorado School of Mines, Golden, Colorado, 2013. (M.S. thesis).
[36] W.C. Oliver, G.M. Pharr, J. Mater. Res. 7 (1992) 1564–1583.
[37] A.C. Fischer-Cripps, Introduction to Contact Mechanics, 2nd ed., Springer Publishing, New York (2007) 78–99.
[38] Q. Ma, D.R. Clarke, J. Mater. Res. 10 (1995) 853–863.
[39] ASTM, Metals Test Methods and Analytical Procedures, ASTM Int., Maryland (2010) 65–71.
[40] D.K. Matlock, F. Zia-Ebrahimi, G. Krauss, Am. Soc. Met. 8205 (1982) 47–87.
[41] B.S. Levy, C.J. Van Tyne, ASM Int. 17 (2008) 842–848.
[42] O.R. Jardim, W.P. Longo, K.K. Chawla, Metallography 17 (1984) 123–130.
[43] J. Kang, Y. Ososkov, J.D. Embury, D.S. Wilkinson, Scr. Mater. 56 (2007) 999–1002.
[44] H. Ghadbeigi, C. Pinna, S. Celotto, J.R. Yates, Mater. Sci. Eng. A. 527 (2010) 5026–5032.
[45] G.E. Dieter, Mechanical Metallurgy, 3rd ed., McGraw-Hill Inc., New York (1986) 222.
[46] D.I. Hyun, S.M. Oak, S.S. Kang, Y.H. Moon, J. Mater. Process. Technol. 130–131 (2002) 9–13.
[47] W. Frącz, F. Stachowicz, T. Trzepieciński, Arch. Civ. Mech. Eng. 12 (2012) 279–283.
[48] N. Pottore, N. Fonstein, I. Gupta, D. Bhattacharya, Iron Steel Technol. 3 (2006) 63–70.
[49] I. Pushkareva, C.P. Scott, M. Gouné, N. Valle, A. Redjaïmia, A. Moulin, ISIJ Int. 53 (2013) 1215–1223.